Carbonation of Serpentinite in Creeping Faults of California

Frieder Klein, David Goldsby, Jian Lin, Muriel Andreani

AGU ADVANCING EARTH AND SPACE SCIENCE

Geophysical Research Letters®

RESEARCH LETTER
10.1029/2022GL099185

Carbonation of Serpentinite in Creeping Faults of California

Frieder Klein[1], David L. Goldsby[2], Jian Lin[1], and Muriel Andreani[3]

[1]Woods Hole Oceanographic Institution, Woods Hole, MA, USA, [2]Department of Earth and Environmental Sciences, University of Pennsylvania, Philadelphia, PA, USA, [3]Laboratoire de Géologie de Lyon, UMR 5276, ENS et Université Lyon 1, Villeurbanne Cedex, France

Key Points:

- Carbonate-altered mantle rocks and CO_2-rich springs are ubiquitous in the creeping section of the San Andreas Fault system
- CO_2-rich spring fluids are saturated with talc and magnesite at seismogenic depths where mineral carbonation is likely ongoing today
- The formation of talc facilitates aseismic creep in wet faults and promotes tectonic movements without large earthquakes

Supporting Information:

Supporting Information may be found in the online version of this article.

Correspondence to:

F. Klein,
fklein@whoi.edu

Citation:

Klein, F., Goldsby, D. L., Lin, J., & Andreani, M. (2022). Carbonation of serpentinite in creeping faults of California. *Geophysical Research Letters*, *49*, e2022GL099185. https://doi.org/10.1029/2022GL099185

Received 19 APR 2022
Accepted 15 JUL 2022

Author Contributions:

Conceptualization: Frieder Klein, David L. Goldsby, Jian Lin
Data curation: Frieder Klein
Formal analysis: Frieder Klein
Funding acquisition: Frieder Klein, David L. Goldsby, Jian Lin
Investigation: Frieder Klein, David L. Goldsby, Jian Lin, Muriel Andreani
Methodology: Frieder Klein
Project Administration: Frieder Klein
Resources: Frieder Klein
Validation: Frieder Klein, Jian Lin
Visualization: Frieder Klein
Writing – original draft: Frieder Klein
Writing – review & editing: Frieder Klein, David L. Goldsby, Jian Lin, Muriel Andreani

Abstract Several large strike slip faults in central and northern California accommodate plate motions through aseismic creep. Although there is no consensus regarding the underlying cause of aseismic creep, aqueous fluids and mechanically weak, velocity-strengthening minerals appear to play a central role. This study integrates field observations and thermodynamic modeling to examine possible relationships between the occurrence of serpentinite, silica-carbonate rock, and CO_2-rich aqueous fluids in creeping faults of California. Our models predict that carbonation of serpentinite leads to the formation of talc and magnesite, followed by silica-carbonate rock. While abundant exposures of silica-carbonate rock indicate complete carbonation, serpentinite-hosted CO_2-rich spring fluids are strongly supersaturated with talc at elevated temperatures. Hence, carbonation of serpentinite is likely ongoing in parts of the San Andres Fault system and operates in conjunction with other modes of talc formation that may further enhance the potential for aseismic creep, thereby limiting the potential for large earthquakes.

Plain Language Summary Constraining the relationships between the mechanical properties of rocks and lubricating fluids in tectonic fault zones is critical to understanding their seismogenic potential. We examined the distribution of exhumed mantle rocks and CO_2-rich springs in the San Andreas Fault area and find ubiquitous evidence for carbonate alteration in the creeping sections. Although carbonate alteration has gone to completion in exposed silica-carbonate rocks, thermodynamic calculations suggest that CO_2-rich spring fluids are supersaturated with talc and magnesite at greater depth where temperatures are high. Because wet talc is a mechanically weak mineral, its formation through carbonation promotes tectonic movements without large earthquakes.

1. Introduction

The San Andreas Fault (SAF) is a right-lateral, strike-slip, transform fault system that accommodates most of the northward motion of the Pacific plate along the western boundary of the North American plate. It is renowned for its large ($M > 7$), infrequent earthquakes on several major fault segments. But a ~150 km-long SAF segment between San Juan Bautista and Parkfield, as well as the northward sister faults of the Calaveras-Hayward system, lack historic earthquakes with $M > 7$. Instead, they are characterized by frequent earthquakes of small to moderate magnitude (M1−4) and high rates (up to 35.9 ± 0.5 mm/yr) of continuous or episodic aseismic creep (Jolivet et al., 2015; Tocher, 1960) (Figure 1). In creeping faults, tectonic strain is released in a quasi-steady motion, thus reducing their potential for large earthquakes. The creeping sections of the SAF do not show any observable heat flow anomaly due to frictional heating, consistent with a model of a mechanically weak fault within strong country rock (Sass et al., 1997). Although there has been little agreement about the underlying mechanisms that cause aseismic creep in the SAF, it appears that aqueous fluids play a critical role (Becken et al., 2011; Irwin & Barnes, 1975; Moore & Lockner, 2013; Pili et al., 2011). A recent magnetotellurics survey identified a deeply rooted zone of anomalously low electric resistivity with connected sub-vertical zones of low resistivity near the SAF northwest of Parkfield, indicating the presence of pathways for considerable quantities of aqueous fluid into the fault (Becken et al., 2011). While a high pore-fluid pressure within the fault would be a simple and plausible means of causing aseismic creep (Fulton & Saffer, 2009; Irwin & Barnes, 1975), the pore pressure within parts of the creeping fault, for example, at the San Andreas Fault Observatory at Depth (SAFOD), is not elevated compared to that of the country rock (Zoback et al., 2011). Another potential cause of aseismic slip is fluid-assisted pressure-solution creep, which has recently been identified in SAFOD samples. This process may account for as much as 20 mm/yr of creep in the SAF (Gratier et al., 2011), but rates of aseismic creep are significantly higher in some parts of the SAF system (Jolivet et al., 2015), calling for an additional or a different mechanism to account

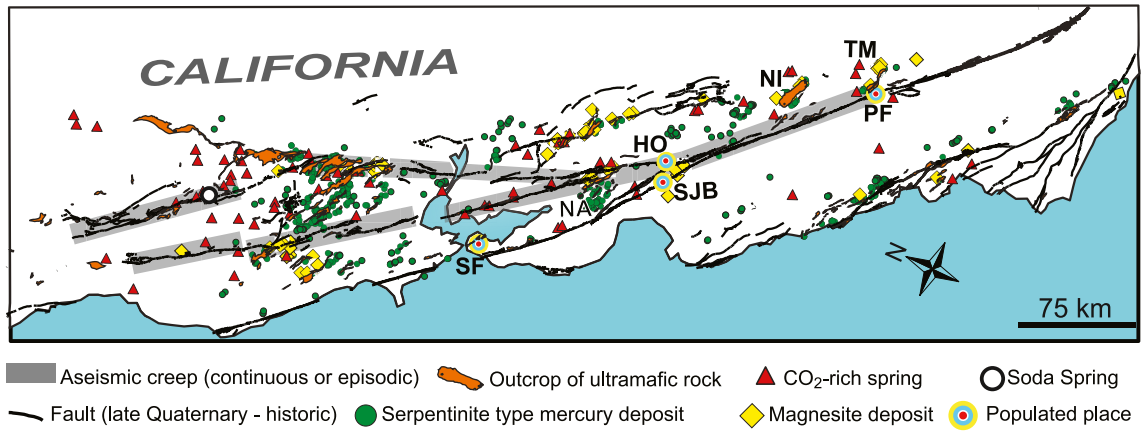

Figure 1. Map illustrating the spatial relationships between numerous serpentinite outcrops, CO_2-rich springs, silica-carbonate rocks and aseismic creep along the San Andreas Fault system. As the dismembered nature of these outcrops suggests, the mapped surface distribution of serpentinite does not necessarily represent its subsurface distribution. In addition to surface outcrops of serpentinite, its presence in the subsurface has been inferred from regional-scale geophysical surveys (McPhee et al., 2004; Watt et al., 2014). Mercury deposits in California are commonly associated with magnesite deposits and silica-carbonate rock, making them a useful indicator for complete carbonation of ultramafic rocks. Mapped outcrops of ultramafic rocks and locations of mineral deposits are from the USGS Mineral Resources database (https://mrdata.usgs.gov/mrds/geo-inventory.php), while locations of CO_2-rich springs are from Irwin and Barnes (1975). SF = San Francisco, SJB San Juan Bautista, HO = Hollister, NI = New Idria, TM = Table Mountain, PF = Parkfield.

for its full extent. The spatial relationship between the occurrence of aseismic creep and outcrops of serpentinite along the SAF and associated sister faults was first recognized in the 1960s (Allen, 1968). Serpentinite exhibits velocity-strengthening behavior at slow slip rates (Reinen et al., 1994). However, the constraints from heat flow and stress orientation of the creeping sections at depths ≥3 km are inconsistent with the high frictional strength of serpentinite at depth as the primary cause for aseismic creep in the SAF (Moore & Rymer, 2007), unless serpentinite is altered to even weaker phyllosilicates (Moore & Lockner, 2013). The low friction coefficients and velocity-strengthening properties of phyllosilicates including talc, saponite and corrensite have recently been found together with serpentine in SAFOD fault gouge (Lockner et al., 2011; Moore, 2014). However, the more abundant corrensite and other clay minerals in the SAFOD fault gouge are stable only at relatively low temperatures, making it unlikely for them to be present at depths greater than 3–4 km (Lockner et al., 2011) where creep rates are highest and talc, chlorite, and amphibole would be stable (Jolivet et al., 2015; Moore et al., 2018).

Fluids infiltrating the SAF system below the seismogenic zone are predominantly a mixture of H_2O and CO_2, as indicated by the compositions of fluids from springs and fluid inclusions (Barnes et al., 1973; Pili et al., 2011). Their isotopic signatures suggest a deep source with contributions from the mantle and from metamorphic devolatilization of crustal lithologies that have been accreted to the western North American margin during collision and subduction of the Farallon plate. Where serpentinite is exposed to CO_2-rich aqueous fluids it can undergo complete carbonation to form silica-carbonate rock (Figure 2, Beinlich et al., 2012; Hansen et al., 2005; Klein & Garrido, 2011; Menzel et al., 2018). But silica-carbonate rock typically does not form directly at the expense of serpentinite, except possibly at very low temperatures (15°C–50°C) where serpentine seems to co-exist stably with quartz (Streit et al., 2012). At higher temperatures carbonation proceeds in a series of dissolution-precipitation reactions that turn serpentinite first into soapstone, a rock that is mainly composed of talc and magnesite, here represented by their simplified Mg-endmembers

$$\underset{\text{serpentine}}{2Mg_3Si_2O_5(OH)_4} + 3CO_{2(aq)} = \underset{\text{talc}}{Mg_3Si_4O_{10}(OH)_2} + \underset{\text{magnesite}}{3MgCO_3} + 3H_2O \quad (1)$$

followed by the formation silica-carbonate rock

$$\underset{\text{talc}}{Mg_3Si_4O_{10}(OH)_2} + 3CO_{2(aq)} = \underset{\text{quartz}}{4SiO_2} + \underset{\text{magnesite}}{3MgCO_3} + H_2O \quad (2)$$

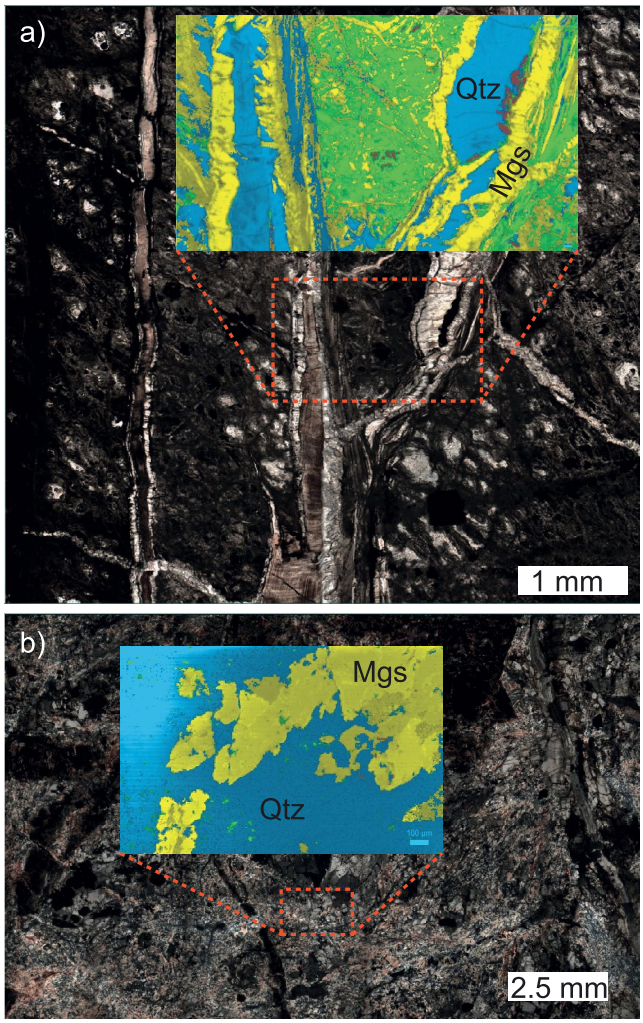

Figure 2. Completely carbonate altered ultramafic rocks composed of magnesite and quartz from New Idria (a) and New Almaden (b). Mosaics of thin section photomicrographs in plane (a) and crossed polarized (b) transmitted light. Inserts are hyperspectral Raman maps depicting the distribution of magnesite (Mgs, yellow), quartz (Qtz, blue), and mixed analyses of poorly crystalline magnesite, quartz, and oxide minerals (green). Few spectra were not identifiable due to a low signal-to-noise ratio (brown). Maps were acquired with a computer-controlled Horiba LabRam HR confocal Raman microscope at Woods Hole Oceanographic Institution using a green (532 nm) laser, 100 µm slit, 150 µm confocal hole, 50% optical filter, 600 grooves/mm grating, and a 100 x objective, and motorized stage. The step size was 5 µm and the acquisition time was 0.6 s per spot. Spectra were processed using LabSpec6 and minerals were identified using the RRUFF spectral library (Downs, 2006).

(Beinlich et al., 2012; Hansen et al., 2005; Klein & Garrido, 2011; Menzel et al., 2018). These and other studies provide firm evidence for the formation of soapstone as an intermediate reaction product that is superseded by silica-carbonate rock (Böhlke, 1989; Griffis, 1972).

It is important to note that reactions 1 and 2 do not require any addition of silica from quartzo-feldspathic country rocks. Instead, the key aqueous species necessary for these reactions to proceed is CO_2, which is strongly enriched in fluids (through metamorphic devolatilization at depth) associated with the SAF system (Barnes et al., 1978). Indeed, in addition to CO_2-rich springs and serpentinite, numerous outcrops of silica-carbonate rock are found between Parkfield and San Juan Bautista and north of Hollister, that is, in parts of the San Andreas fault system where rates of aseismic creep are highest (Figure 1). Prominent examples of silica-carbonate rock exposures include the Mount Jackson, Culver-Baer, and New Almaden mines, which represent mercury deposits of (past) economic value (Bailey et al., 1973). Henderson (1969) referred to these mineralizations as "serpentinite type mercury deposits." Countless mercury deposits in California are associated with ultramafic rocks (Figure 1) and their distribution can be used as a proxy for silica-carbonate alteration. Likewise, the numerous magnesite deposits associated with ultramafic rocks are another indicator of silica-carbonate alteration (Figure 1). Both mercury and magnesite mineralizations appear to align with the direction of faulting in California and faults represent major pathways for CO_2-rich aqueous fluids (Figure 1). While most magnesite surface deposits were formed in the geological past, locations of CO_2-rich springs associated with ultramafic rocks may pinpoint sites of ongoing carbonation in the San Andreas Fault zone at depth.

2. Fluid Speciation and Reaction Path Modeling

Speciation calculations and reaction path models were computed using CO_2-rich fluids from Soda Spring fluids (39°24'27.3"N 122°58'22.0"W), Wilbur Springs (39°02'19.3"N 122°25'14.9"W), and Seigler Springs (38°52'33.6"N 122°41'16.8"W) reported in Barnes et al. (1973). We used the software code EQ3/6, version 8.0 with a customized thermodynamic database for aqueous species, pure minerals, and solid solutions assembled using the software code SUPCRT92 (Helgeson et al., 1978; Johnson et al., 1992; Klein et al., 2009, 2013; McCollom, 2000; Shock & Helgeson, 1988; Shock et al., 1989; Wolery, 1992; Wolery & Jove-Colon, 2004). The EQ3/6 database contains log K values for temperatures from 0°C to 400°C in 25°C increments. Geothermal gradients in the SAF are relatively well constrained in the Parkfield area and range from 27 to 40°C/km (Williams et al., 2004), suggesting that the temperature of fluids entering the SAF near the base of the crust may be as high as 600°C. The depth of the seismogenic zone varies from less than 10 km in the Geysers-Clear Lake area to 15 km between San Juan Bautista and Parkfield. Accordingly, temperatures of fluids in the seismogenic zone are likely between ~100°C and 400°C, depending on the local geothermal gradient. The speciation calculations and reaction path models depicted in Figure 3 were calculated assuming a maximum geothermal gradient of 40°C/km at hydrostatic conditions within the fault. For example, at 200°C this corresponds to 5 km depth and a hydrostatic pressure of 50 MPa. To facilitate comparison of saturation states of predicted mineralogies at different temperatures, all models were calculated for a constant pressure of 50 MPa. Because changes in pressure below 100 MPa have a negligible effect on equilibrium constants, small changes in temperature can compensate changes in pressure (Klein & Garrido, 2011). We used the B-dot equation with hard-core diameter and B-dot and Debye–Hückel parameters from reference

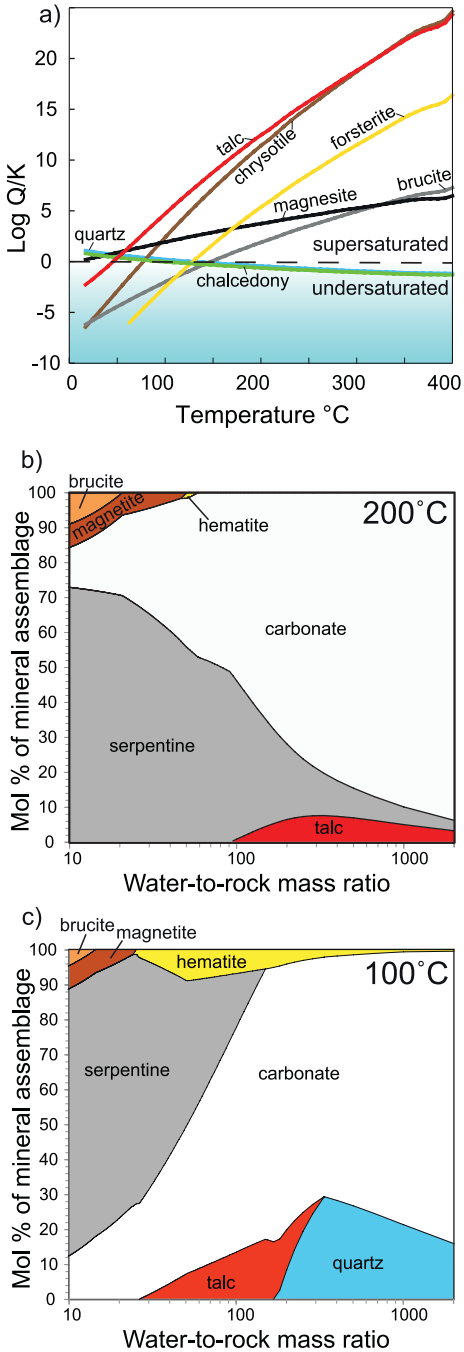

Figure 3. Modeling results illustrating the interactions between CO_2-rich fluids and serpentinite in the San Andreas Fault (SAF). (a) Calculated saturation indices (log Q/K) for minerals in fluids from Soda Spring as a function of temperature using published fluid data (Barnes et al., 1973). (b and c) Predicted equilibrium mineral assemblage for the reaction of heated Soda Spring fluid with serpentinized peridotite as a function of the water-to-rock mass ratio (*w*/*r*) at 100°C and 200°C. Low *w*/*r* represents rock-dominated zones away from a fault, whereas high w/*r* represents fluid dominated zones closer to a fault (cf. Figure S1 in Supporting Information S1). For similar models that capture serpentinization reactions at lower *w*/*r*, please refer to Klein et al. (2009, 2013).

(Wolery & Jove-Colon, 2004). Activity coefficients for neutral species were set to one, except for non-polar gaseous species, for which the activity coefficients of CO_2 (Drummond, 1981) were adopted. Solid solutions used in the thermodynamic reaction path models include the primary minerals olivine (with the end-members forsterite and fayalite), orthopyroxene (enstatite and ferrosilite), and clinopyroxene (diopside and hedenbergite), as well as the secondary minerals serpentine (chrysotile, greenalite, kaolinite, cronstedtite), brucite (Mg-brucite and ferroan brucite), talc (talc and minnesotaite). The composition of the solid starting material used for the reaction path models is 80 mol% olivine (molar forsterite:fayalite = 9:1), 10 mol % orthopyroxene (enstatite:ferrosilite = 9:1), and 10 mol% clinopyroxene (diopside:hedenbergite = 9:1). The Soda Spring fluid composition was speciated at 17°C and then heated to 100°C and 200°C at 50 MPa. Solid reactant was added in small increments to the heated fluid to assess changes in the predicted equilibrium mineral assemblage for water-to-rock mass ratios (*w*/*r*) between 10 and 2000 (Figure 3).

3. Talc Saturation and Soapstone Formation at Depth

We elucidate possible connections among serpentinite, CO_2-rich aqueous fluids, and silica-carbonate rock in the creeping sections of the SAF system using thermodynamic calculations. First, we calculated the saturation states of major minerals found in serpentinite, soapstone and silica-carbonate rock for aqueous fluids from Soda Spring at elevated temperatures (Figure 2a) to assess whether carbonation is an ongoing process at seismogenic depths within the fault. Consistent with previous results, our calculations suggest that spring fluids are saturated with quartz and magnesite (i.e., silica-carbonate rock) at ambient surface temperatures (Barnes et al., 1973). However, at temperatures between 50°C and 400°C talc is the most strongly supersaturated mineral, suggesting that it is the most likely mineral to precipitate. Between 50°C and 100°C magnesite is the second most supersaturated mineral. Other supersaturated minerals at higher temperatures are serpentine, olivine, and brucite. For comparison, we also calculated the saturation states of minerals in aqueous fluids from Wilbur and Seigler springs, which yield essentially the same results, with talc being the most supersaturated mineral at temperatures between ca. 50°C and 400°C.

To further assess fluid-rock interactions at depth, we computed two reaction path models for the reaction between heated Soda Spring fluid and serpentinized peridotite at 100°C and 200°C (Figures 3b and 3c). In rock-dominated domains away from major fluid pathways, the predicted equilibrium mineral assemblage is dominated by serpentine with minor amounts of brucite, Ca-rich carbonate, and magnetite at both temperatures. Where fluid supply is high such as in veins and faults, the amount of serpentine decreases while Mg-rich carbonate and talc become the dominant minerals. At low temperatures, talc and carbonate (solid solution dominated by the magnesite component) represent a transient mineral assemblage and the reaction runs to completion forming silica-carbonate rock. These results strongly suggest that carbonation is an ongoing process and that soapstone indeed could form in the SAF at depth. However, at low temperatures, soapstone is an ephemeral reaction product within the alteration sequence, suggesting that it is not abundant or only temporarily present at shallow depth, consistent with the dominance of completely altered silica-carbonate rock in surface outcrops (Figure 1).

4. Carbonation of Serpentinite and Aseismic Creep

The widespread occurrence of silica-carbonate rock and its close association with serpentinite, and talc-saturated CO_2-rich springs in the San Andreas fault system provide compelling evidence for talc-formation due to mineral carbonation at the present day as well as in the geologic past. Talc is widely believed to be one of the weakest minerals in fault zones (Escartín et al., 2008; Moore & Lockner, 2008); however, depending on the availability of water, the frictional properties of talc are highly variable. Whereas water-saturated talc has a low fiction coefficient $\mu = 0.1–0.3$ and pronounced velocity-strengthening behavior, room-dry talc has a significantly higher friction coefficient $\mu = 0.4–1$ and velocity neutral or weakening behavior (Chen et al., 2017). Wet talc-bearing faults and their dry equivalents likely show contrasting seismic properties. Because heat flow measurements along the creeping sections of the San Andreas fault system constrain the apparent coefficient of friction of the fault to 0.2 or less (d'Alessio et al., 2006), wet, talc-bearing faults could satisfy the strength limitations and explain the aseismic slip whereas dry talc could not. Its high frictional strength coefficient and velocity neutral or weakening behavior could indeed facilitate earthquakes. While it seems rather unlikely that active San Andreas faults are dry, the mechanical properties of completely silica-carbonate altered serpentinite may enable frequent earthquakes of small to moderate magnitude (den Hartog et al., 2014; Toppozada et al., 2002).

Because CO_2-rich aqueous fluids and ultramafic rocks are particularly common in young orogenic belts and subduction zones (Barnes et al., 1978; Coleman, 1977; Reynard, 2013), the formation of talc via mineral carbonation may play a critical role in controlling the seismic behavior of major tectonic faults around the world.

Data Availability Statement

The data that support the findings of this study are freely available from the United States Geological Survey Mineral Resource Data System (https://mrdata.usgs.gov/mrds/geo-inventory.php). Locations of CO_2-rich springs are from Irwin and Barnes (1975, http://doi.org/10.1130/0091–7613(1975)3<713:EOGSAM>2.0.CO;2). The compositions of CO_2-rich spring fluids used for speciation calculations and reaction path models are from Barnes et al. (1973, https://doi.org/10.2113/gsecongeo.68.3.388). The model input and output files for this research are freely available at https://doi.org/10.5281/zenodo.6470879.

Acknowledgments
This work was supported by National Science Foundation (NSF) grants NSF-EAR-1220280 to F. K. and J. L., NSF-EAR-1219908 to D. G., and NSF-OCE-2001728 to J. L. We are grateful for constructive reviews by Diane Moore and Jacob Tielke and thank Quentin Williams for editorial handling.

References

Allen, C. R. (1968). *The tectonic environments of seismically active and inactive areas along the San Andreas Fault system* (pp. 70–82). Stanford University Publications, Geological Sciences.

Bailey, E. H., Clark, A. L., & Smith, R. M. (1973). United States mineral resources: Mercury. *U. S. Geological Survey Professional Paper*, *820*, 401–414.

Barnes, I., Irwin, W. P., & White, D. E. (1978). *Global distribution of carbon dioxide discharges, and major fault zones of seismicity: U.S* (pp. 78–39). Geological Survey Water-Resources Investigations.

Barnes, I., O'Neil, J. R., Rapp, J. B., & White, D. E. (1973). Silica-carbonate alteration of serpentinite: Wall rock alteration in mercury deposits of the California Coastal ranges. *Economic Geology*, *68*(3), 388–398. https://doi.org/10.2113/gsecongeo.68.3.388

Becken, M., Ritter, O., Bedrosian, P. A., & Weckmann, U. (2011). Correlation between deep fluids, tremor and creep along the central San Andreas Fault. *Nature*, *480*(7375), 87–90. https://doi.org/10.1038/nature10609

Beinlich, A., Plümper, O., Hövelmann, J., Austrheim, H., & Jamtveit, B. (2012). Massive serpentinite carbonation at Linnajavri, N–Norway. *Terra Nova*, *24*(6), 446–455. https://doi.org/10.1111/j.1365-3121.2012.01083.x

Böhlke, J. K. (1989). Comparison of metasomatic reactions between a common CO_2-rich vein fluid and diverse wall rocks; intensive variables, mass transfers, and Au mineralization at Alleghany, California. *Economic Geology*, *84*, 291–327. https://doi.org/10.2113/gsecongeo.84.2.291

Chen, X., Elwood Madden, A. S., & Reches, Z. (2017). The frictional strength of talc gouge in high-velocity shear experiments. *Journal of Geophysical Research: Solid Earth*, *122*(5), 3661–3676. https://doi.org/10.1002/2016JB013676

Coleman, R. G. (1977). *Ophiolites: Ancient oceanic lithosphere?* (p. 229). Springer Verlag.

d'Alessio, M. A., Williams, C. F., & Bürgmann, R. (2006). Frictional strength heterogeneity and surface heat flow: Implications for the strength of the creeping San Andreas Fault. *Journal of Geophysical Research*, *111*(B5), B05410. https://doi.org/10.1029/2005JB003780

den Hartog, S. A., Saffer, D. M., & Spiers, C. J. (2014). The roles of quartz and water in controlling unstable slip in phyllosilicate-rich megathrust fault gouges. *Earth Planets and Space*, *66*, 78. https://doi.org/10.1186/1880-5981-66-78

Downs, R. T. (2006). The RRUFF Project: An integrated study of the chemistry, crystallography, Raman and infrared spectroscopy of minerals.

Drummond, S. E., Jr. (1981). *Boiling and mixing of hydrothermal fluids: Chemical effects on mineral precipitation*. The Pennsylvania State University.

Escartín, J., Andreani, M., Hirth, G., & Evans, B. (2008). Relationships between the microstructural evolution and the rheology of talc at elevated pressures and temperatures. *Earth and Planetary Science Letters*, *268*(3–4), 463–475. https://doi.org/10.1016/j.epsl.2008.02.004

Fulton, P. M., & Saffer, D. M. (2009). Potential role of mantle-derived fluids in weakening the San Andreas Fault. *Journal of Geophysical Research*, *114*(B7), B07408. https://doi.org/10.1029/2008JB006087

Gratier, J.-P., Richard, J., Renard, F., Mittempergher, S., Doan, M.-L., Di Toro, G., et al. (2011). Aseismic sliding of active faults by pressure solution creep: Evidence from the San Andreas Fault observatory at depth. *Geology*, *39*(12), 1131–1134. https://doi.org/10.1130/G32073.1

Griffis, R. (1972). Genesis of a magnesite deposit, Deloro Twp., Ontario. *Economic Geology*, *67*(1), 63–71. https://doi.org/10.2113/gsecongeo.67.1.63

Hansen, L. D., Dipple, G. M., Gordon, T. M., & Kellett, D. A. (2005). Carbonated serpentinite (listwanite) at Atlin, British Columbia: A geological analogue to carbon dioxide sequestration. *The Canadian Mineralogist*, *43*(1), 225–239. https://doi.org/10.2113/gscanmin.43.1.225

Helgeson, H. C., Delany, J. M., Nesbitt, H. W., & Bird, D. K. (1978). Summary and critique of the thermodynamic properties of rock-forming minerals. *American Journal of Science*, *278A*, 1–229.

Henderson, F. B. (1969). Hydrothermal alteration and ore deposition in serpentinite-type mercury deposits. *Economic Geology*, *64*(5), 489–499. https://doi.org/10.2113/gsecongeo.64.5.489

Irwin, W. P., & Barnes, I. (1975). Effect of geologic structure and metamorphic fluids on seismic behaviour of San-Andreas Fault system in central and northern California. *Geology*, *3*(12), 713–716. //A1975AX38200010. https://doi.org/10.1130/0091-7613(1975)3<713:eogsam>2.0.co;2

Johnson, J. W., Oelkers, E. H., & Helgeson, H. C. (1992). SUPCRT92: A software package for calculating the standard molal thermodynamic properties of minerals, gases, aqueous species, and reactions from 1–5000 bars and 0–1000°C. *Computers & Geosciences*, *18*(7), 899–947. https://doi.org/10.1016/0098-3004(92)90029-q

Jolivet, R., Simons, M., Agram, P. S., Duputel, Z., & Shen, Z. K. (2015). Aseismic slip and seismogenic coupling along the central San Andreas Fault. *Geophysical Research Letters*, *42*(2), 297–306. https://doi.org/10.1002/2014gl062222

Klein, F., Bach, W., Jöns, N., McCollom, T., Moskowitz, B., & Berquó, T. (2009). Iron partitioning and hydrogen generation during serpentinization of abyssal peridotites from 15°N on the Mid-Atlantic Ridge. *Geochimica et Cosmochimica Acta*, *73*(22), 6868–6893. https://doi.org/10.1016/j.gca.2009.08.021

Klein, F., Bach, W., & McCollom, T. M. (2013). Compositional controls on hydrogen generation during serpentinization of ultramafic rocks. *Lithos*, *178*, 55–69. https://doi.org/10.1016/j.lithos.2013.03.008

Klein, F., & Garrido, C. J. (2011). Thermodynamic constraints on mineral carbonation of serpentinized peridotite. *Lithos*, *126*(3–4), 147–160. https://doi.org/10.1016/j.lithos.2011.07.020

Lockner, D. A., Morrow, C., Moore, D., & Hickman, S. (2011). Low strength of deep San Andreas Fault gouge from SAFOD core. *Nature*, *472*(7341), 82–85. https://doi.org/10.1038/nature09927

McCollom, T. M. (2000). Geochemical constraints on primary productivity in submarine hydrothermal vent plumes. *Deep-Sea Research Letters*, *47*(1), 85–101. https://doi.org/10.1016/s0967-0637(99)00048-5

McPhee, D. K., Jachens, R. C., & Wentworth, C. M. (2004). Crustal structure across the San Andreas Fault at the SAFOD site from potential field and geologic studies. *Geophysical Research Letters*, *31*(12). https://doi.org/10.1029/2004GL019363

Menzel, M. D., Garrido, C. J., López Sánchez-Vizcaíno, V., Marchesi, C., Hidas, K., Escayola, M. P., & Delgado Huertas, A. (2018). Carbonation of mantle peridotite by CO_2-rich fluids: The formation of listvenites in the Advocate ophiolite complex (Newfoundland, Canada). *ABYSS*, *323*, 238–261. https://doi.org/10.1016/j.lithos.2018.06.001

Moore, D. E. (2014). Comparative mineral chemistry and textures of SAFOD fault gouge and damage-zone rocks. *Journal of Structural Geology*, *68*, 82–96. Part A. https://doi.org/10.1016/j.jsg.2014.09.002

Moore, D. E., & Lockner, D. A. (2008). Talc friction in the temperature range 25°–400°C: Relevance for fault-zone weakening. *Tectonophysics*, *449*(1–4), 120–132. https://doi.org/10.1016/j.tecto.2007.11.039

Moore, D. E., & Lockner, D. A. (2013). Chemical controls on fault behavior: Weakening of serpentinite sheared against quartz-bearing rocks and its significance for fault creep in the San Andreas system. *Journal of Geophysical Research: Solid Earth*, *118*(5), 2558–2570. https://doi.org/10.1002/jgrb.50140

Moore, D. E., McLaughlin, R. J., & Lienkaemper, J. J. (2018). Serpentinite-rich gouge in a creeping segment of the Bartlett Springs Fault, northern California: Comparison with SAFOD and implications for seismic hazard. *Tectonics*, *37*(12), 4515–4534. https://doi.org/10.1029/2018TC005307

Moore, D. E., & Rymer, M. J. (2007). Talc-bearing serpentinite and the creeping section of the San Andreas Fault. *Nature*, *448*(7155), 795–797. https://doi.org/10.1038/nature06064

Pili, É., Kennedy, B. M., Conrad, M. E., & Gratier, J.-P. (2011). Isotopic evidence for the infiltration of mantle and metamorphic CO_2–H_2O fluids from below in faulted rocks from the San Andreas Fault system. *Chemical Geology*, *281*(3–4), 242–252. https://doi.org/10.1016/j.chemgeo.2010.12.011

Reinen, L., Weeks, J., & Tullis, T. (1994). The frictional behavior of lizardite and antigorite serpentinites: Experiments, constitutive models, and implications for natural faults. *Pure and Applied Geophysics*, *143*(1–3), 317–358. https://doi.org/10.1007/BF00874334

Reynard, B. (2013). Serpentine in active subduction zones. *Lithos*, *178*, 171–185. https://doi.org/10.1016/j.lithos.2012.10.012

Sass, J. H., Williams, C. F., Lachenbruch, A. H., Galanis, S. P., Jr., & Grubb, F. V. (1997). Thermal regime of the San Andreas Fault near Parkfield, California. *Journal of Geophysical Research*, *102*(B12), 27575–27585. https://doi.org/10.1029/JB102iB12p27575

Shock, E. L., & Helgeson, H. C. (1988). Calculation of the thermodynamic and transport properties of aqueous species at high pressures and temperatures: Correlation algorithms for ionic species and equation of state predictions to 5 kb and 1000°C. *Geochimica et Cosmochimica Acta*, *52*(8), 2009–2036. https://doi.org/10.1016/0016-7037(88)90181-0

Shock, E. L., Helgeson, H. C., & Sverjensky, D. A. (1989). Calculation of the thermodynamic and transport properties of aqueous species at high pressures and temperatures: Standard partial molal properties of inorganic neutral species. *Geochimic et Cosmochimica Acta*, *53*(9), 2157–2183. https://doi.org/10.1016/0016-7037(89)90341-4

Streit, E., Kelemen, P., & Eiler, J. (2012). Coexisting serpentine and quartz from carbonate-bearing serpentinized peridotite in the Samail Ophiolite, Oman. *Contributions to Mineralogy and Petrology*, *164*, 821–837. https://doi.org/10.1007/s00410-012-0775-z

Tocher, D. (1960). Creep on the San Andreas Fault: Creep rate and related measurements at Vineyard, California. *Bulletin of the Seismological Society of America*, *50*(3), 389–415.

Toppozada, T. R., Branum, D. M., Reichle, M. S., & Hallstrom, C. L. (2002). San Andreas Fault zone, California: M ≥ 5.5 earthquake history. *Bulletin of the Seismological Society of America*, *92*(7), 2555–2601. https://doi.org/10.1785/0120000614

Watt, J. T., Ponce, D. A., Graymer, R. W., Jachens, R. C., & Simpson, R. W. (2014). Subsurface geometry of the San Andreas-Calaveras fault junction: Influence of serpentinite and the Coast range ophiolite. *Tectonics*, *33*(10), 2025–2044. https://doi.org/10.1002/2014TC003561

Williams, C. F., Grubb, F. V., & Galanis, S. P., Jr. (2004). Heat flow in the SAFOD pilot hole and implications for the strength of the San Andreas Fault. *Geophysical Research Letters*, *31*(15), L15S14. https://doi.org/10.1029/2003GL019352

Wolery, T. J. (1992). *EQ3/6, A software package for geochemical modeling of aqueous systems: Package overview and installation guide (version 7.0)*. Lawrence Livermore National Laboratory.

Wolery, T. J., & Jove-Colon, C. F. (2004). *Qualification of thermodynamic data for geochemical modeling of mineral-water interactions in dilute systems: U.S. Department of energy report, ANL-WIS--GS-000003 REV00* (p. 212). Bechtel SAIC Company, LLC, Las Vegas, Nevada. https://doi.org/10.2172/850412

Zoback, M., Hickman, S., & Ellsworth, W., & SAFOD Science Team. (2011). Scientific drilling into the San Andreas Fault zone—An overview of SAFOD's first five years. *Scientific Drilling*, *11*, 14–28. https://doi.org/10.5194/sd-11-14-2011